Effect of Extended Thiophene Segments in Small Band Gap Polymers with Thienopyrazine

Arjan P. Zoombelt, Jan Gilot, Martijn M. Wienk, and René A. J. Janssen*

Molecular Materials and Nanosystems, Eindhoven University of Technology, P.O. Box 513, 5600 MB Eindhoven, The Netherlands, and Dutch Polymer Institute (DPI), P.O. Box 902, 5600 AX Eindhoven, The Netherlands

Received January 20, 2009. Revised Manuscript Received March 7, 2009

Three new small band gap polymers were synthesized and applied in bulk heterojunction solar cells together with [60]PCBM and [70]PCBM. The polymers are based on quarterthiophene or quinquethiophene segments alternating with thienopyrazine units along the chain and were obtained via Yamamoto or Suzuki polymerization. In thin solid films, the band gaps vary from 1.3 to 1.5 eV. All polymers give a photoresponse up to 850 nm when combined with a methanofullerene derivative. The best cells gave a power conversion efficiency of 1.4% under simulated standard solar light conditions (AM1.5, 100 mW/cm^2).

Introduction

The discovery of bulk heterojunction solar cells stimulated research in small band gap π-conjugated polymers.[1−11] Designed to absorb a large part of the solar spectrum, these *p*-type polymers (donor) can be applied in organic solar cells in combination with a methanofullerene derivative as an *n*-type material (acceptor). The small band gap of the polymer leads to an enhanced absorption and potentially increases photocurrent. The most widely used strategy to make small band gap polymers involves incorporation of electron-rich (donor) and electron-deficient (acceptor) units in an alternating fashion in a polymer chain.[3,9,12−21] The energy levels of the polymer depend on the chemical nature of the donor and acceptor units, where the highest occupied molecular orbital (HOMO) is mainly governed by the donor, while the electron affinity of the acceptor predominantly determines the lowest unoccupied molecular orbital (LUMO) position.[22,23]

It is important to control the energy levels of the polymer, since it is generally considered that the LUMO−LUMO offset between the polymer and fullerene directly relates to the charge separation efficiency. It is suggested that a minimum LUMO−LUMO offset of ∼0.3−0.4 eV is required to ensure quantitative charge separation at the donor/acceptor interface.[24,25] On the other hand, the energy difference between the HOMO of the donor and the LUMO of the acceptor determines the maximum attainable open circuit voltage (V_{oc}) of the solar cell and in consequence directly affects maximum power output.[26,27] Hence, it is crucial to judiciously position the energy levels of the polymer with respect to the acceptor to ensure quantitative charge separation and a high V_{oc}, while maintaining a small band gap.

* Corresponding author. E-mail: r.a.j.janssen@tue.nl.

(1) Halls, J. J. M.; Walsh, C. A.; Greenham, N. C.; Marseglia, E. A.; Friend, R. H.; Moratti, S. C.; Holmes, A. B. *Nature (London)* **1995**, *376*, 498–500.
(2) Yu, G.; Gao, J.; Hummelen, J. C.; Wudl, F.; Heeger, A. J. *Science* **1995**, *270*, 1789–1791.
(3) Dhanabalan, A.; Van Duren, J. K. J.; Van Hal, P. A.; Van Dongen, J. L. J.; Janssen, R. A. J. *Adv. Funct. Mater.* **2001**, *11*, 255–262.
(4) Shaheen, S. E.; Vangeneugden, D.; Kiebooms, R.; Vanderzande, D.; Fromherz, T.; Padinger, F.; Brabec, C. J.; Sariciftci, N. S. *Synth. Met.* **2001**, *121*, 1583–1584.
(5) Brabec, C. J.; Winder, C.; Sariciftci, N. S.; Hummelen, J. C.; Dhanabalan, A.; Van Hal, P. A.; Janssen, R. A. J. *Adv. Funct. Mater.* **2002**, *12*, 709–712.
(6) Muhlbacher, D.; Neugebauer, H.; Cravino, A.; Sariciftci, N. S. *Synth. Met.* **2003**, *137*, 1361–1362.
(7) Henckens, A.; Knipper, M.; Polec, I.; Manca, J.; Lutsen, L.; Vanderzande, D. *Thin Solid Films* **2004**, *451−452*, 572–579.
(8) Wang, X.; Perzon, E.; Delgado, J. L.; De la Cruz, P.; Zhang, F.; Langa, F.; Andersson, M.; Inganas, O. *Appl. Phys. Lett.* **2004**, *85*, 5081–5083.
(9) Campos, L. M.; Tontcheva, A.; Guenes, S.; Sonmez, G.; Neugebauer, H.; Sariciftci, N. S.; Wudl, F. *Chem. Mater.* **2005**, *17*, 4031–4033.
(10) Peet, J.; Kim, J. Y.; Coates, N. E.; Ma, W. L.; Moses, D.; Heeger, A. J.; Bazan, G. C. *Nat. Mater.* **2007**, *6*, 497–500.
(11) Wienk, M. M.; Turbiez, M.; Gilot, J.; Janssen, R. A. J. *Adv. Mater.* **2008**, *20*, 2556–2560.
(12) Mühlbacher, D.; Scharber, M.; Morana, M.; Zhu, Z.; Waller, D.; Gaudiana, R.; Brabec, C. *Adv. Mater.* **2006**, *18*, 2884–2889.
(13) Perzon, E.; Wang, X.; Admassie, S.; Inganaes, O.; Andersson, M. R. *Polymer* **2006**, *47*, 4261–4268.
(14) Wienk, M. M.; Struijk, M. P.; Janssen, R. A. J. *Chem. Phys. Lett.* **2006**, *422*, 488–491.
(15) Wienk, M. M.; Turbiez, M.; G, R.; Struijk, M. P.; Fonrodona, M.; Janssen, R. A. J. *Appl. Phys. Lett.* **2006**, *88*, 153511/1–153511/3.
(16) Bundgaard, E.; Krebs, F. C. *Sol. Energy Mater. Sol. Cells* **2007**, *91*, 954–985.
(17) Roncali, J. *Chem. Rev.* **1997**, *97*, 173–205.
(18) Bundgaard, E.; Krebs, F. C. *Macromolecules* **2006**, *39*, 2823–2831.
(19) Zhu, Y.; Champion, R. D.; Jenekhe, S. A. *Macromolecules* **2006**, *39*, 8712–8719.
(20) Wang, E.; Wang, L.; Lan, L.; Luo, C.; Zhuang, W.; Peng, J.; Cao, Y. *Appl. Phys. Lett.* **2008**, *92*, 033307/1–033307/3.
(21) Hou, J.; Chen, H.-Y.; Zhang, S.; Li, G.; Yang, Y. *J. Am. Chem. Soc.* **2008**, *130*, 16144–16145.
(22) Ajayaghosh, A. *Chem. Soc. Rev.* **2003**, *32*, 181–191.
(23) van Mullekom, H. A. M.; Vekemans, J. A. J. M.; Havinga, E. E.; Meijer, E. W. *Mater. Sci. Eng., R: Reports* **2001**, *R32*, 1–40.
(24) Koster, L. J. A.; Mihailetchi, V. D.; Blom, P. W. M. *Appl. Phys. Lett.* **2006**, *88*, 093511/1–093511/3.
(25) Scharber, M. C.; Mühlbacher, D.; Koppe, M.; Denk, P.; Waldauf, C.; Heeger, A. J.; Brabec, C. J. *Adv. Mater.* **2006**, *18*, 789–794.
(26) Gadisa, A.; Svensson, M.; Andersson, M. R.; Inganas, O. *Appl. Phys. Lett.* **2004**, *84*, 1609–1611.
(27) Brabec, C. J.; Cravino, A.; Meissner, D.; Sariciftci, N. S.; Fromherz, T.; Rispens, M. T.; Sanchez, L.; Hummelen, J. C. *Adv. Funct. Mater.* **2001**, *11*, 374–380.

10.1021/cm900184z CCC: $40.75
Published on Web 04/01/2009

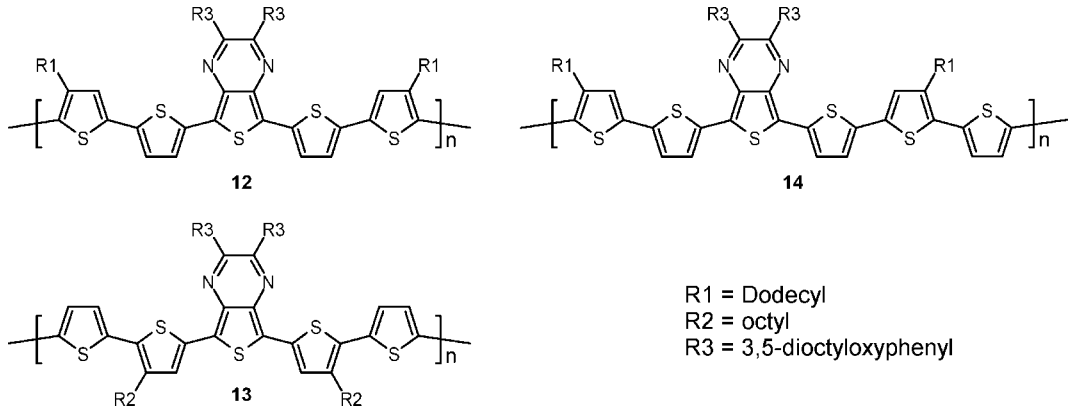

Figure 1. Small band gap polymers based on alternating thienopyrazine and either quarterthiophene (**12**, **13**) or quinquethiophene (**14**) units.

Scheme 1. Synthetic Route Towards Monomers 10 and 11

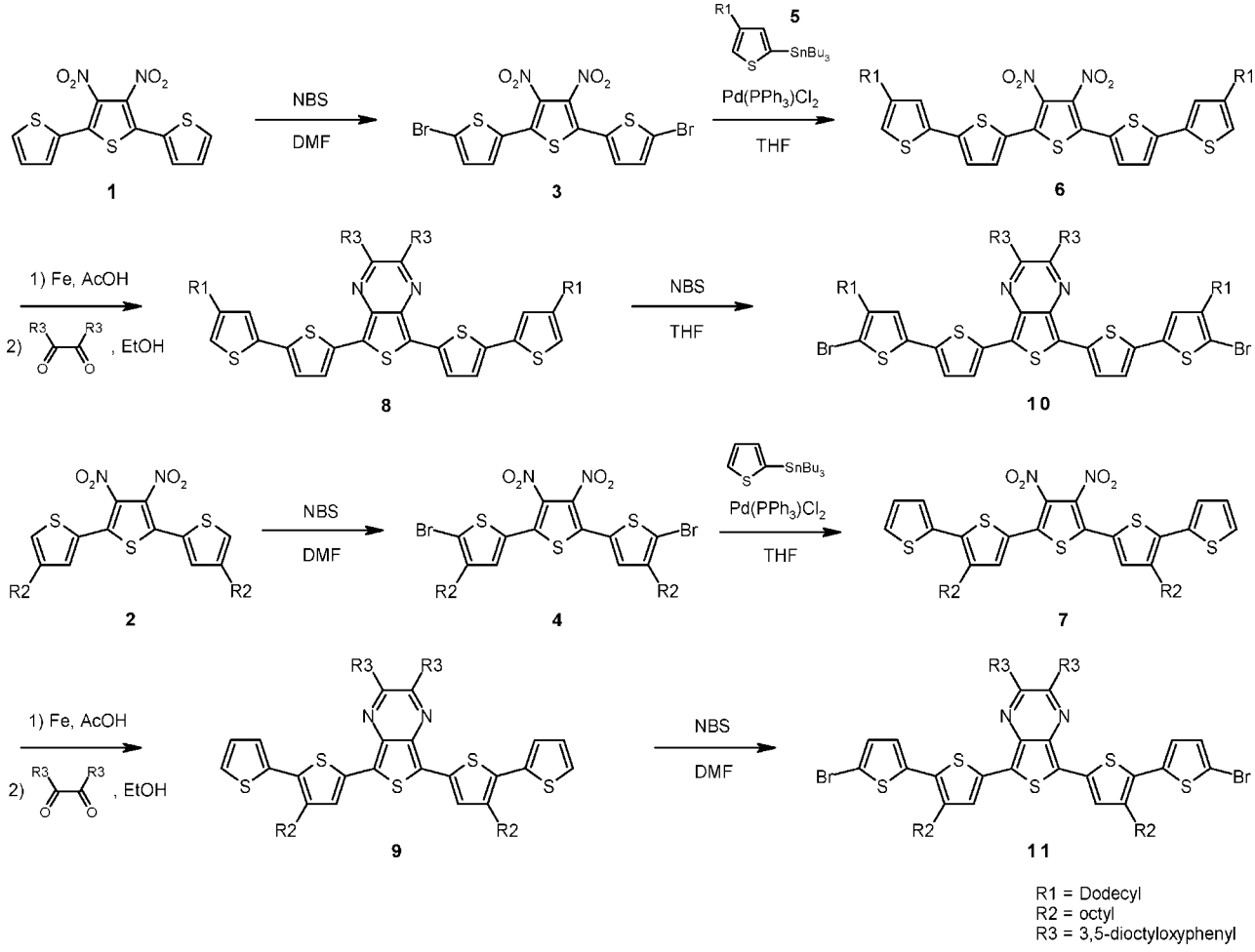

Here we report on the synthesis of three new small band gap polymers and their photovoltaic performance together with methanofullerenes [60]PCBM and [70]PCBM (i.e., the [6,6]-phenyl C_{61} and C_{71} butyric acid methyl esters). The polymers, shown in Figure 1, are based on thienopyrazine alternating with quarterthiophene or quinquethiophene segments along the chain. In earlier work,[15] we discussed the properties and photovoltaic performance of polymers based on thienopyrazine and bithiophene. Here the length of the thiophene units is increased, and their influence on (photo)-physical properties is investigated. Furthermore, the effect of planarity is investigated by varying the position of the alkyl side chains.

Experimental Section

The synthetic procedures for preparing monomers and polymers and their characterization by ^{1}H and ^{13}C NMR are described in detail in the Supporting Information. Molecular weights were determined using size exclusion chromatography in HPLC-grade *o*-dichlorobenzene (ODCB) at 80 °C against polystyrene standards on a Polymer Laboratories-GPC 120 high temperature chromatograph, a PD 2040 high-temperature light scattering detector, and a

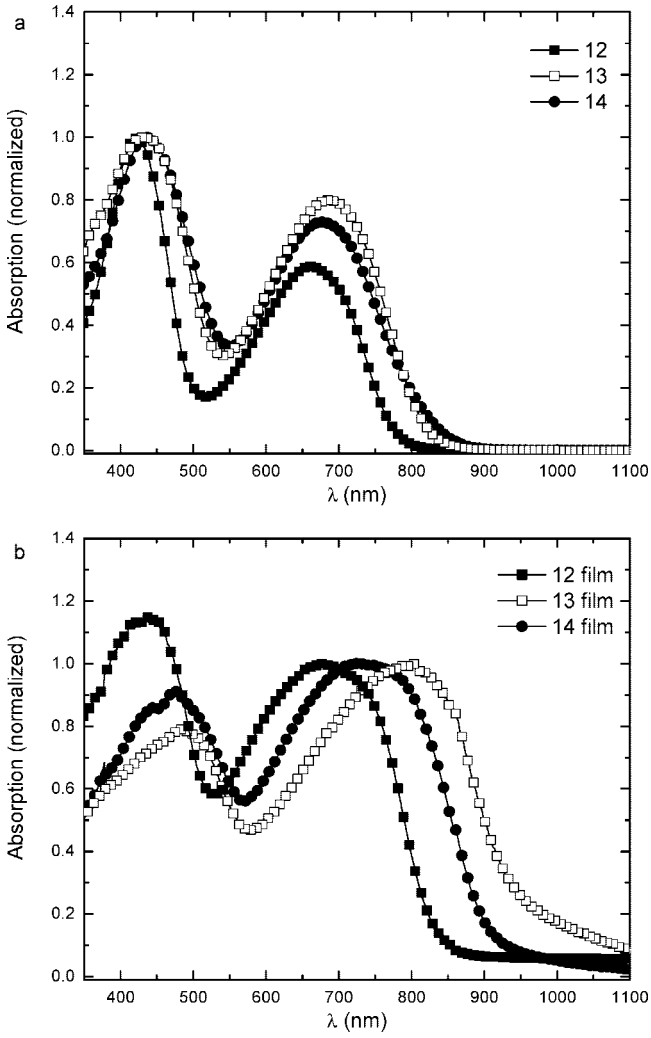

Figure 2. Room temperature UV−vis absorption spectra of the polymers (a) in OBCB solution and (b) as thin films.

Midas autosampler. A mixed-C 300 × 7.5 mm column was used, together with a precolumn. The flow rate was 1 mL/min and the injection volume 100 μL.

UV−vis absorption spectra were measured with a Perkin-Elmer Lambda 900 spectrometer. Cyclic voltammetry (scan rate = 100 mV/s) was performed on an Autolab PGSTAT30 potentiostat in a three-electrode single-compartment cell using ODCB containing 0.1 M $TBAPF_6$ (Fluka) as electrolyte. The working electrode was platinum disk, the counter electrode a silver rod, and the reference electrode Ag/AgCl. Potentials are relative to Fc/Fc^+ used as an internal standard.

Photovoltaic devices were made by spin coating PEDOT:PSS (Clevios P, VP Al4083) onto precleaned, patterned indium tin oxide (ITO) substrates (14 Ω per square) (Naranjo Substrates). The photoactive layer was deposited by spin coating from the appropriate solvent. The counter electrode of LiF (1 nm) and aluminum (100 nm) was deposited by vacuum evaporation at 3×10^{-7} mbar. The active area of the cells was 0.16 cm^2. $J-V$ characteristics were measured under ~100 mW/cm^2 white light from a tungsten-halogen lamp filtered by a Schott GG385 UV filter and a Hoya LB120 daylight filter, using a Keithley 2400 source meter. Spectral response was measured under operation conditions using bias light from a 532 nm solid state laser (Edmund Optics). Monochromatic light from a 50 W tungsten halogen lamp (Philips focusline) in combination with monochromator (Oriel, Cornerstone 130) was modulated with a mechanical chopper. The response was recorded as the voltage over a 50 Ω resistance, using a lock-in amplifier (Stanford research Systems SR830). A calibrated Si cell was used as reference. The device was kept behind a quartz window in a nitrogen filled container. Short circuit currents under AM1.5 conditions were obtained from the spectral response and convolution with the solar spectrum (J_{sc}(SR)). The value of J_{sc}(SR) was used with V_{oc} and FF from the 100 mW/cm^2 white light $J-V$ characteristics to estimate the power conversion efficiency η. This procedure gives values in close correspondence to those obtained from a solar simulator and taking into account the spectral mismatch correction.[11]

Tapping mode AFM was measured in a NanoScope Dimension 3100 microscope (Veeco, Digital Instruments) or in a MFP-3D (Asylum Research) using PPP-NCHR probes (Nanosensors).

Results and Discussion

Synthesis. The synthesis route toward monomers **10** and **11** is depicted in Scheme 1. Applying 2 equiv of *N*-bromosuccinimide in tetrahydrofuran (THF) at 50 °C to either 3′,4′-dinitroterthiophene (**1**)[28] or 4,4″-dioctyl-3′,4′-dinitro[2,2′;5′,2″]terthiophene (**2**)[28] afforded **3** and **4**, respectively, as orange solids after precipitation in methanol. Stille coupling of **3** with 2-tributylstannyl-4-dodecylthiophene (**5**) using bis(triphenylphosphine)palladium(II) dichloride [$Pd(PPh_3)Cl_2$] gave quinquethiophene **6** in 50% yield. An identical procedure for **4** and 2-tributylstannylthiophene resulted in quinquethiophene **7** in 94% yield. The somewhat lower yield for **6** is very likely due to a negative steric influence during the transmetalation step of the alkyl substituted stannylthiophene **5**. It has been shown that steric hindrance can have a profound influence on the effectiveness of C−C cross coupling reactions.[29] The dinitro-derivatives **6** and **7** were reduced with iron dust in acetic acid to the corresponding diamines. Both diamines were subjected, without purification, to condensation coupling with 1,2-bis(3,5-dioctyloxyphenyl)ethanedione in ethanol giving **8** and **9** in 50% yield over 2 steps. To allow polymerization via Yamamoto coupling, compounds **8** and **9** were dibrominated using *N*-bromosuccinimide in either THF or DMF. Electrophilic substitution at the α-position of **8** proceeded with high selectivity and yield due to the electron donating dodecyl side chains located at the 3 and 3′′′′ positions. However, halogenation of **9** resulted in a mixture of mono-, di-, tri-, and tetrabrominated species, since here the alkyl chains on the 4′ and 4′′′ position reduce selectivity by increasing reactivity toward electrophilic aromatic substitution of the β-positions on the outer thiophene ring. Using the more polar DMF instead of THF provided a somewhat higher selectivity, but extensive column chromatography was needed to separate all components and obtain pure **11**.

Yamamoto coupling of **10**, using bis(1,5-cyclooctadiene)nickel(0) [$Ni(cod)_2$] and bipyridine (Scheme 2), gave head-to-head (HH) coupled polymer **12** as a green solid with a molecular weight (M_w) of 131 kg/mol and a polydispersity (PDI) of 2.8. Polymerization of **11**, using an identical procedure as for **10**, afforded **13** as a green polymer with M_w = 230 kg/mol and PDI = 3.1.

(28) Kitamura, C.; Tanaka, S.; Yamashita, Y. *Chem. Mater.* **1996**, *8*, 570–578.
(29) Schroeter, S.; Stock, C.; Bach, T. *Tetrahedron* **2005**, *61*, 2245–2267.

Table 1. Optical and Electrochemical Data of the Polymers in ODCB and in Thin Films[a]

	solution							film		
polymer	λ_{max} (nm)	λ_{onset} (nm)	E_g (eV)	$\varepsilon(\lambda_{max})$ (L/(g·cm))	E^{ox}_{onset} (V)	E^{red}_{onset} (V)	E^{cv}_g (eV)	λ_{max} (nm)	λ_{onset} (nm)	E_g (eV)
12	661	776	1.60	17	0.10	−1.58	1.68	676	820	1.50
13	687	817	1.52	23	–0.07	−1.57	1.50	801	937	1.32
14	677	820	1.51	25	0.01	−1.55	1.56	724	904	1.37
PCBM		709	1.75			−1.07				

[a] Electrochemical potentials (vs Fc/Fc^+) in ODCB containing 0.1 M $TBAPF_6$ (scan rate = 100 mV/s, concentration 2×10^{-3} M based on monomer units).

Table 2. Photovoltaic Performance of Blends of Small Band Gap Polymers with Methanofullerenes

polymer	acceptor	solvent	layer thickness (nm)	V_{oc} (V)	J_{sc}(SR) (mA/cm^2)	FF	η (%)
12	[60]PCBM	ODCB/$CHCl_3$	114	0.71	3.02	0.42	0.90
	[70]PCBM	ODCB	54	0.74	3.85	0.58	1.37
13	[60]PCBM	CB	95	0.60	3.15	0.44	0.83
	[70]PCBM	ODCB	62	0.63	5.45	0.41	1.41
14	[60]PCBM	ODCB/$CHCl_3$	77	0.62	2.10	0.59	0.77
	[70]PCBM	ODCB	63	0.63	3.01	0.57	1.08

To prevent the HH coupling in **12** and further increase the donor content in these donor−acceptor small band gap polymers, **10** was copolymerized via Suzuki cross coupling with 2,5-bis-thiopheneboronic acid pinacol ester. Polymer **14** was obtained as a green solid with M_w = 30 kg/mol and PDI = 3.4 (Scheme 3).

Optical Properties. The absorption spectra of the polymers dissolved in *o*-dichlorobenzene are shown in Figure 2a. The optical gaps, defined by the onset of absorption, are rather similar varying between 1.5 and 1.6 eV (Table 1). The presence of HH coupling in **12** results in a larger optical gap (1.6 eV) due to a twisted backbone that reduces the

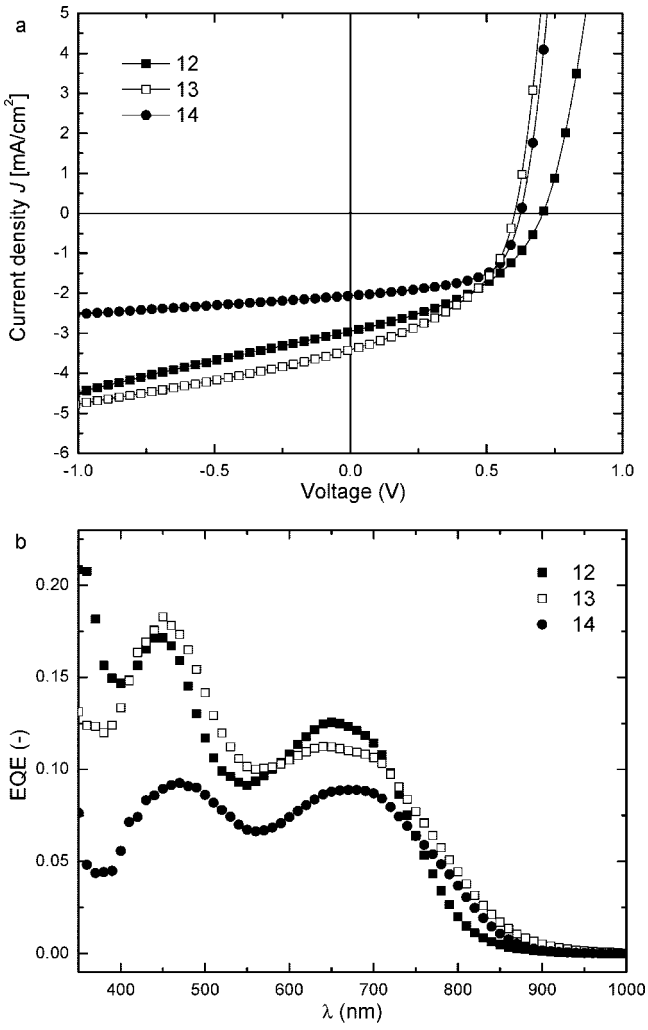

Figure 3. (a) *J*−*V* curves of polymer:[60]PCBM solar cells under 100 mW/cm^2 white light illumination. (b) Monochromatic EQE of polymer:[60]PCBM solar cells.

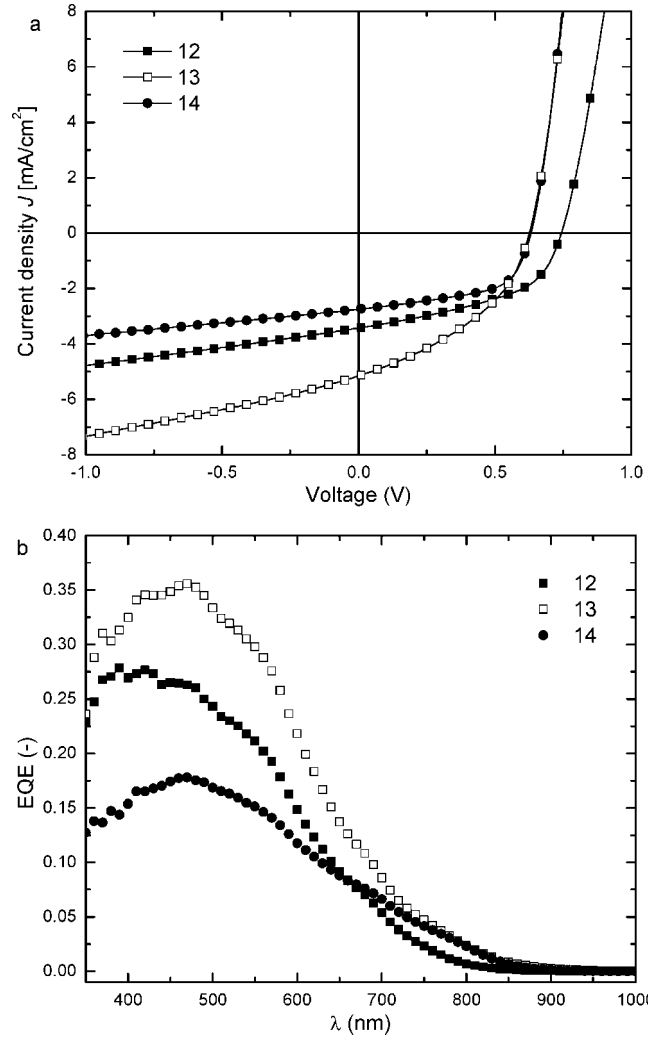

Figure 4. (a) *J*−*V* curves of polymer:[70]PCBM solar cells under 100 mW/cm^2 white light illumination. (b) Monochromatic EQE of polymer:[70]PCBM solar cells.

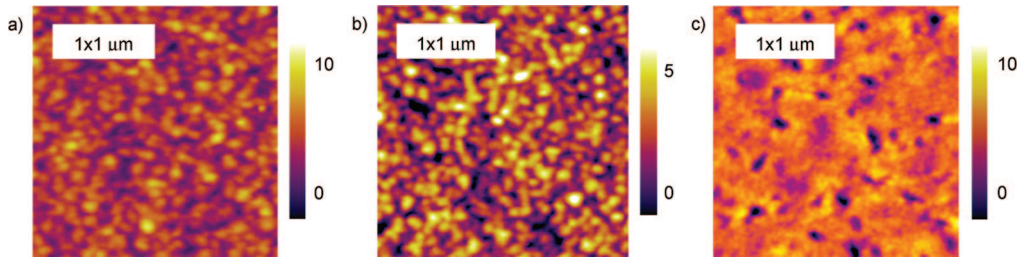

Figure 5. AFM height images of [60]PCBM blended with (a) **12** and (b) **13** spin coated from ODCB/$CHCl_3$ and CB, respectively, and with (c) **14** spin coated from ODCB/$CHCl_3$.

Scheme 2. Yamamoto Polymerization of 10 and 11

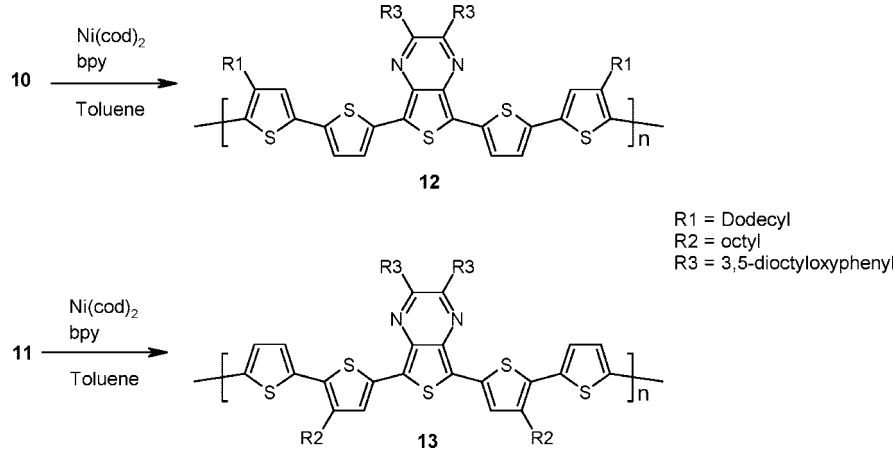

Scheme 3. Suzuki Copolymerization of 10 and 2,5-Bis-thiopheneboronic Acid Pinacol Ester Using $Pd_2(dba)_3$

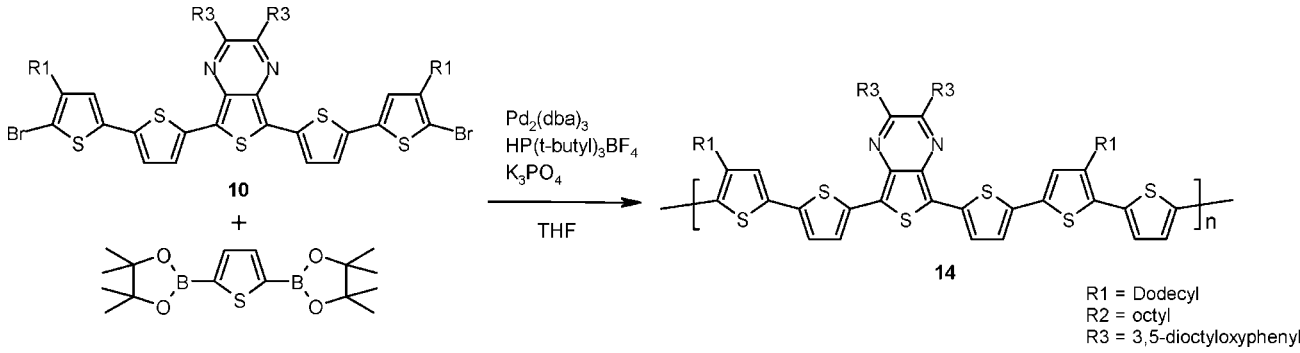

overlap of the π-orbitals and the conjugation. Consequently, the absence of HH coupling in polymers **13** and **14** gives rise to somewhat smaller optical gaps of 1.52 and 1.51 eV, respectively. Compared to alternating thiophene−thienopyrazine polymers with a shorter bithiophene segment,[15,19] the optical gap of the polymers with the quaterthiophene and quinquethiophene units increases from 1.3 to 1.5−1.6 eV, despite electron donating alkyl side chains. The optical gap is reduced to values below 1 eV for a homopolymer of thienopyrazine,[30] showing that increasing the number of thienopyrazines reduces the optical gap,[31] while it increases with the number of thiophene rings.

The difference in absorption maxima (λ_{max}), listed in Table 1, is relatively small but does show a bathochromic shift when a more planar configuration is allowed. The λ_{max} of **13** and **14** are red-shifted by 26 and 16 nm, respectively, compared to λ_{max} = 661 nm for polymer **12** (Figure 2a). The twisted backbone in **12** also lowers the extinction coefficient compared to the other polymers (Table 1). However, the effect of planarization is best reflected in the solid state absorption spectra, depicted in Figure 2b. Where **12** exhibits a red shift in absorption maximum of only 15 nm, polymers **13** and **14** show bathochromic shifts of 114 and 47 nm, respectively. Also the onset of absorption in the solid state of **13** is furthest red-shifted to 937 nm, setting its band gap at 1.32 eV.

Electrochemistry. Cyclic voltammetry was performed (see Supporting Information) for each polymer dissolved in ODCB, and the results are collected in Table 1. The electrochemical gap is determined as the difference between the onsets of the oxidation and reduction potentials ($E_g^{cv} = E_{onset}^{ox} - E_{onset}^{red}$) and is in good agreement with the optical gap (E_g) determined in solution. The reduction potential of the polymers is virtually identical for all polymers, varying only between −1.55 and −1.58 V (vs Fc/Fc^+). Since the

(30) Wen, L.; Duck, B. C.; Dastoor, P. C.; Rasmussen, S. C. *Macromolecules* **2008**, *41*, 4576–4578.
(31) Karsten, B. P.; Janssen, R. A. J. *Org. Lett.* **2008**, *10*, 3513–3516.

LUMO is more localized on the electron-deficient unit,[32] thienopyrazine, it seems to be less affected by conformational changes in the polymer backbone due to HH coupling. Conversely, the oxidation potential is influenced by the planarity of the thiophene rings and might therefore also alter the maximum attainable V_{oc}. For polymer **12**, HH coupling increases the oxidation potential by decreasing the conjugation and, hence, can possibly lead to a higher V_{oc}. Incorporating an additional unsubstituted thiophene ring, in the case of **14**, allows a more planar structure and results in a decrease of E^{ox}_{onset} by almost 100 mV. Clearly, placing two unsubstituted thiophenes next to each other, as in polymer **13**, further reduces E^{ox}_{onset} by 70 mV to −0.07 V (vs Fc/Fc^+). This means that the V_{oc} for **13** might be approximately 200 mV lower than in the case of **12**, but a planar conformation might lead to closer packing in the solid state and thus provide higher current densities since charge carrier mobility is expected to increase when order increases.[33,34]

Solar Cells. The polymers were applied in bulk heterojunction solar cells with either [60]PCBM or [70]PCBM as electron acceptor. The active layers were spin coated onto an indium tin oxide (ITO) covered glass substrate covered by a 60 nm film of PEDOT:PSS. LiF (1 nm) and Al (100 nm) were thermally evaporated as back electrode. Generally, spin coating the polymer/PCBM mixture in a ratio 1:4 (by weight) from either chlorobenzene (CB), ODCB, or a chloroform ($CHCl_3$)−ODCB mixture (4:1, v/v), with a polymer concentration of 5 mg/mL, afforded the best photovoltaic performance.

The optimized solar cell efficiencies are summarized in Table 2. As was expected from the oxidation potentials, polymer **12**:[60]PCBM cells spin coated from ODCB/$CHCl_3$ have the highest V_{oc} of about 0.71 V. The current density was $J_{sc} = 2.95$ mA/cm^2 (Figure 3a) under 100 mW/cm^2 white light illumination. Convolution of the spectral response (SR) (Figure 3b) with the AM1.5 spectrum affords an estimate of $J_{sc}(SR) = 3.02$ mA/cm^2 under standard solar light conditions (AM1.5, 100 mW/cm^2). Together with a fill factor of FF = 0.42, the cells give an estimated efficiency of $\eta = 0.9\%$. The spectrally resolved external quantum efficiency (EQE, i.e., the number of charges collected at short circuit per incident photon) is shown in Figure 3b. Polymer **12**:[60]PCBM gives an EQE up to ∼12% in the 550−750 nm range and extends to approximately 850 nm. The EQE of polymer **13**:[60]PCBM is somewhat lower with a quantum efficiency of about 10% in the 550−750 nm range, but it does show a photoresponse up to almost 900 nm. This slightly increased the current for polymer **13**:[60]PCBM cells spin coated from CB compared to **12**, providing $J_{sc} = 3.41$ mA/cm^2 [estimated AM1.5 $J_{sc}(SR) = 3.15$ mA/cm^2]. The V_{oc} of polymer **13**:[60]PCBM cells was lower at 0.60 V, which is in fair agreement with the optical and electrochemical data (Table 1). The fill factor was limited to 0.44 resulting in an overall estimated power conversion efficiency of $\eta = 0.83\%$. The highest fill factor of 0.59 was achieved for polymer **14**:[60]PCBM cells. All cells show an increased photocurrent at reversed bias (Figure 3a), suggesting field assisted collection of charges. This effect is most pronounced for **12** and **13**, while for **14** the majority of created charges reaches the electrodes already at short circuit. Nevertheless, the short-circuit current for **14** is lower compared to the other polymers, being $J_{sc} = 2.06$ mA/cm^2 [estimated AM1.5 $J_{sc}(SR) = 2.10$ mA/cm^2], indicating that free charge carrier generation or collection is inferior. It might be that charge dissociation is inefficient or that charge recombination is relatively fast compared to transport and reduces short-circuit current. Together with a V_{oc} of 0.62 V the energy conversion efficiency of polymer **14**:[60]PCBM solar cells was estimated at 0.77%.

The EQE of the polymer:[60]PCBM cells all have an onset at ∼850 nm and show a first maximum at ∼650 nm (Figure 3b). The absorption spectra of the polymer films (Figure 2b), however, appear more red-shifted, especially for **13** and **14**. The explanation for this difference is the reduced tendency for polymer chains to spontaneously order and aggregate in mixtures with PCBM. As a consequence the EQE curves more closely resembles the absorption spectrum of the polymer in solution as can be seen by comparing Figures 2a and 3b. This effect has previously been described in some detail for polythiophenes mixed with PCBM,[35] and it relates to the fact that P3HT:[60]PCBM films require annealing to reach their maximum performance.[36]

The field-effect hole mobilities, μ, are 1.6×10^{-4}, 1.0×10^{-3}, and 1.2×10^{-5} cm^2/(V s) for **12**, **13**, and **14**, respectively (see Supporting Information). These values show little or no direct correlation with the photovoltaic performance of the blends, and further work would be required to determine whether charge generation, recombination, or transport and collection limits the device performance for the device shown in Table 2.

The $J-V$ curves and external quantum efficiencies of the polymers with [70]PCBM are depicted in Figure 4a,b, respectively. [70]PCBM has similar electrochemical properties to [60]PCBM, but it absorbs more light in the visible region owing to its lower symmetry that causes the dipole forbidden transition to become (partly) allowed.[37] The additional absorption in the visible region can increase the photocurrent, significantly, up to 50%.[37] The active layers were spin coated from ODCB with a polymer:[70]PCBM ratio of 1:4. Incorporating [70]PCBM resulted in a performance increase of about 50% for all polymers. The effect of [70]PCBM is clearly visible in the external quantum efficiency (Figure 4b). The main enhancement, with EQEs reaching 35% for polymer **13**:[70]PCBM, is in the 400−600 nm range, where [70]PCBM absorbs. At the same time the

(32) Karsten, B. P.; Viani, L.; Gierschner, J.; Cornil, J.; Janssen, R. A. J. *J. Phys. Chem. A* **2008**, *112*, 10764–10773.
(33) McCulloch, I.; Heeney, M.; Bailey, C.; Genevicius, K.; MacDonald, I.; Shkunov, M.; Sparrowe, D.; Tierney, S.; Wagner, R.; Zhang, W.; Chabinyc, M. L.; Kline, R. J.; McGehee, M. D.; Toney, M. F. *Nat. Mater.* **2006**, *5*, 328–333.
(34) Chabinyc, M. L.; Toney, M. F.; Kline, R. J.; McCulloch, I.; Heeney, M. *J. Am. Chem. Soc.* **2007**, *129*, 3226–3237.
(35) Cremer, J.; Wienk, M. M.; Janssen, R. A. J.; Bäuerle, P. *Chem. Mater.* **2006**, *18*, 5832–5834.
(36) Padinger, F.; Rittberger, R. S.; Sariciftci, N. S. *Adv. Funct. Mater.* **2003**, *13*, 85.
(37) Wienk, M. M.; Kroon, J. M.; Verhees, W. J. H.; Knol, J.; Hummelen, J. C.; van Hal, P. A.; Janssen, R. A. J. *Angew. Chem., Int. Ed.* **2003**, *42*, 3371–3375.

contribution of the polymer to the photocurrent decreases at long wavelengths. This is likely a consequence of the different optimal layer thickness for the incoupling of visible and NIR light, caused by interference in the cell. As can be seen in Table 2, the optimized layer thickness for devices based on **12** and **13** with [70]PCBM is less than for devices with [60]PCBM, consistent with the fact that for visible light the first interference maximum of absorbed photons is found at lower film thickness than for NIR light. For **14**, the difference in optimized active layer thickness in blends with [60]PCBM and [70]PCBM is small, and also the EQEs are similar in the NIR region. Since the electron mobilities in [60]PCBM and [70]PCBM are similar[38] and higher than that of the polymers, a mobility difference is not likely to cause the difference in optimal layer thickness.

Polymer **13**:[70]PCBM cells showed the best performance with J_{sc}(SR) = 5.45 mA/cm^2, V_{oc} = 0.63 V, and a FF of 0.41; the power conversion efficiency increased to 1.41%.

Morphology. The efficiency in bulk heterojunction solar cells is for a large part determined by morphology.[39−44] Creating an interpenetrating network of the donor and acceptor material is crucial to obtain a large interfacial area ensuring quantitative charge separation. In addition, percolating pathways are required to allow efficient transport of free charge carriers to the electrodes. It is thus important to control morphology of the active layer and make sure that the performance is not limited by a coarse scale phase separation.

In Figure 5, atomic force microscopy (AFM) height images of **12**:[60]PCBM (Figure 5a), **13**:[60]PCBM (Figure 5b), and **14**:[60]PCBM (Figure 5c) are shown for the optimized devices listed in Table 2. Similar images were recorded for the corresponding polymer:[70]PCBM blends (see Supporting Information). All blends form relatively smooth films with little height difference. Figure 5a,b show small features up to several nanometers in diameter when processed from ODCB/$CHCl_3$ or CB, respectively: a size small enough for a large donor/acceptor interface and sufficiently large for percolating pathways to exist. The absence of features with a size larger than 100 nm indicates that the blends do not suffer from extensive demixing. Spin coating from other solvents like CB or ODCB resulted in either too large or too small phase separation (see Supporting Information). The **14**:[60]PCBM blend exhibits a rather homogeneous layer when spin coated from ODCB/$CHCl_3$. Spin coating from solvents like $CHCl_3$ or CB resulted in an even more homogeneous material distribution (see Supporting Information), possibly limiting charge carrier transport to the electrodes. The reduced current densities of these devices might be a direct consequence of that.

Conclusions

In summary, three new small band gap polymers were synthesized consisting of alternating thienopyrazine units and either quarterthiophene or quinquethiophene segments. The polymers were obtained in relatively high molecular weight. The position of the alkyl substituents on the thiophene backbone was varied to fine-tune (photo)physical properties. Introducing HH coupling resulted in a larger optical and electrochemical gaps due to a loss in planarity. The optical gap decreases by ∼100 meV in solution to almost 200 meV in solid state when a more planar structure is allowed. Polymer **13** has the smallest band gap of 1.32 eV in thin film. The main change in band gap is due to a shift in oxidation potential, that is, the HOMO level of the polymer. This difference in E_{onset}^{ox} is also reflected in V_{oc} with **12** producing over 0.7 V, while the V_{oc} for the more planar **13** is limited to ∼0.6 V. However, overall performance was nearly identical with estimated efficiencies of about 0.9% with [60]PCBM and up to 1.4% with [70]PCBM. Generally, a higher J_{sc} for **13** compensated for the loss in V_{oc}. The use of [70]PCBM instead of [60]PCBM increases the performance for all polymers, due to additional absorption of [70]PCBM in the visible region of the spectrum.

Acknowledgment. We thank Simon Mathijssen for measurements of charge carrier mobilities and Zhenglei Zhang for assistance with solar cell optimization. This work is part of the research program of the Dutch Polymer Institute (DPI, Project 524).

Supporting Information Available: Experimental procedures for the synthesis of the monomers and polymers according to Schemes 1, 2, and 3, optical absorption spectra of the monomers, cyclic voltammograms, and AFM images of the polymer:PCBM blends (PDF). This material is available free of charge via the Internet at http://pubs.acs.org.

CM900184Z

(38) Wobkenberg, P. H.; Bradley, D. D. C.; Kronholm, D.; Hummelen, J. C.; de Leeuw, D. M.; Colle, M.; Anthopoulos, T. D. *Synth. Met.* **2008**, *158*, 468–472.
(39) Van Duren, J. K. J.; Yang, X.; Loos, J.; Bulle-Lieuwma, C. W. T.; Sieval, A. B.; Hummelen, J. C.; Janssen, R. A. J. *Adv. Funct. Mater.* **2004**, *14*, 425–434.
(40) Hoppe, H.; Sariciftci, N. S. *J. Mater. Chem.* **2006**, *16*, 45–61.
(41) Yang, X.; Loos, J. *Macromolecules* **2007**, *40*, 1353–1362.
(42) Hoppe, H.; Niggemann, M.; Winder, C.; Kraut, J.; Hiesgen, R.; Hinsch, A.; Meissner, D.; Sariciftci, N. S. *Adv. Funct. Mater.* **2004**, *14*, 1005–1011.
(43) Liu, J.; Shi, Y.; Yang, Y. *Adv. Funct. Mater.* **2001**, *11*, 420–424.
(44) Mammo, W.; Admassie, S.; Gadisa, A.; Zhang, F.; Inganaes, O.; Andersson, M. R. *Sol. Energy Mater. Sol. Cells* **2007**, *91*, 1010–1018.